Determining the mixing of oil and sea water using polarimetric synthetic aperture radar

Brent Minchew[1]

Received 8 May 2012; revised 15 July 2012; accepted 16 July 2012; published 23 August 2012.

[1] Knowledge of the characteristics of spilled oil in the ocean is important for cleanup operations, predictions of the impact on wildlife, and studies of the nature of the ocean surface and currents. Herein I discuss a method for evaluating the characteristics of oil in a marine environment using synthetic aperture radar (SAR) and present a new, simple classification, called the oil/water mixing index (Mdex), to quickly assess the results. I link the Mdex results to the Bonn Agreement for Oil Appearance Codes (BAOAC) for aerial observers and demonstrate the Mdex on Uninhabited Aerial Vehicle SAR (UAVSAR) data collected June 23, 2010 over the former site of the Deepwater Horizon (DWH) drilling rig. The Mdex map shows a more heterogeneous oil swath than do radar backscatter images and features within the oil are consistent with features present in previously published, near-coincident optical imagery. The Mdex results indicate that most of the oil near the DWH was mixed with sea water to a minimum depth of a few millimeters, though some areas containing relatively thin films are observed. **Citation:** Minchew, B. (2012), Determining the mixing of oil and sea water using polarimetric synthetic aperture radar, *Geophys. Res. Lett.*, *39*, L16607, doi:10.1029/2012GL052304.

1. Introduction

[2] Large oil spills in marine environments rank among the worst man-made calamities. Mitigating the environmental damage caused by oil spills requires prompt and effective cleanup operations which, in turn, require consistent reliable information on the whereabouts and general properties of the oil. Moreover, observations of oil spills provide data on ocean currents, wind-wave interactions, the behavior of surface contaminants, and the potential effect on wildlife. Given the shear size of some oil spills, remote sensing methods may be the only effective means of gathering synoptic-scale observations of the spill.

[3] It has long been known that marine oil spills are visible as areas of low backscatter power in synthetic aperture radar (SAR) images [e.g., *Wright*, 1966; *Valenzuela*, 1978; *Gade et al.*, 1998; *Jones et al.*, 2011]. There are two ways oil can reduce the SAR backscatter power. First, oil can reduce the small-scale wind-driven surface roughness, relative to uncontaminated sea water under the same environmental conditions, causing a smaller percentage of the reflected radar energy to be directed back to the radar antenna. Second, if oil is mixed in high enough concentrations within a thin layer (a few millimeters for a radar wavelength of 24 cm) below the surface, the oil will reduce the effective dielectric constant of the ocean surface because the dielectric constant of oil is much lower than that of sea water. A lower dielectric constant means less total energy will be reflected by the surface.

[4] Many studies have focused on the use of SAR to identify oil on open water [e.g., *Gade et al.*, 1998; *Solberg et al.*, 1999; *Fiscella et al.*, 2000; *Brekke and Solberg*, 2008]. These studies generally either ignore the characteristics of the oil, preferring instead to focus on identifying oil and distinguishing it from false positives, or are predicated on the assumption that oil exists only in thin surface layers. However, oil is known to mix with water through wave action and weathering and oil properties can change over timescales of hours to days due to loss of volatiles, emulsification, entrainment of sediment, and other weathering processes [e.g., *National Research Council*, 2003]. Recent work has suggested that SAR is sensitive to the characteristics of oil [*Jones et al.*, 2011] and it has been demonstrated that polarimetric SAR can be used to infer the mixing of oil and sea water [*Minchew et al.*, 2012].

[5] In this study, I expand the method for decoupling the effects of reduced dielectric constant and damping of the surface roughness first demonstrated by *Minchew et al.* [2012] and apply a simple classification to the results in order to infer if and to what extent oil may be mixed with sea water near the surface and whether oil is manifest on the surface as a viscoelastic film. I link the new classification, hereafter called the oil/water mixing index (Mdex), to the Bonn Agreement for Oil Appearance Codes (BAOAC) for aerial observers of oil spills [*NOAA*, 2007] in order to describe the physical properties of the oil and promulgate a common communication mode for optical and SAR observations. Data acquired by the Uninhabited Aerial Vehicle Synthetic Aperture Radar (UAVSAR) on June 23, 2010 over the former Deepwater Horizon (DWH) site provides an illustrative case for the Mdex. Given the proximity of the data to the DWH and the severity of the spill, the criteria $\sigma_{VV}^{o(water)}/\sigma_{VV}^{o} > 1.2$, where σ_{VV}^{o} represents the observed backscatter power and $\sigma_{VV}^{o(water)}$ the along-track mean values of areas deemed to be relatively clean water, indicates crude oil contamination.

2. Methodology

2.1. Scattering From the Ocean Surface

[6] Radar backscatter power is proportional to the normalized radar cross section (NRCS) which can be modeled for the ocean surface under moderate wind conditions by

[1]Seismological Laboratory, Division of Geological and Planetary Sciences, California Institute of Technology, Pasadena, California, USA.

Corresponding author: B. Minchew, Seismological Laboratory, California Institute of Technology, 1200 E. California Blvd., MS 252-21, Pasadena, CA 91125, USA. (bminchew@caltech.edu)

0094-8276/12/2012GL052304

considering the ocean to be composed of small, slightly rough facets that are tilted relative to local up. The facet tilt is governed by long-wavelength ocean waves and the superimposed small-scale roughness represents wind-driven gravity-capillary waves. The gravity-capillary waves that correspond to the well-known Bragg wavenumber $k_{Bragg} = 2k_r\sin\theta_i$, where θ_i is the radar incidence angle and k_r is the radar wavenumber in free space, are the primary contributors to the SAR backscatter.

[7] The orientation of the facet normal in the radar reference frame is defined by two angles: ψ, which is the angle between local up and the projection of the facet normal onto the radar scattering plane (the vertically oriented plane that contains the radar line-of-sight), and ζ, which is the angle between local up and the projection of the facet normal onto the vertically oriented plane perpendicular to the scattering plane (typically this plane contains the platform velocity vector). Taking into account ψ and ζ, the incidence angle of the radar with respect to the facet is $\theta_i = \cos^{-1}[\cos(\theta + \psi)\cos(\zeta)]$ where θ is the angle of incidence relative to local (untilted) up. Then the co-polarized NRCS is given as:

$$\sigma^0_{pp} = 4\pi k_r^4 \cos^4\theta_i \Gamma_{pp} W \tag{1}$$

where the subscript *pp* indicates either *HH* or *VV* polarizations [*Valenzuela*, 1968; *Valenzuela et al.*, 1971; *Valenzuela*, 1978]. The integral of the radiated power over all reflection angles is described by the reflectivity $\Gamma_{pp} = \Gamma_{pp}(\varepsilon_r, \theta_i)$ where ε_r is the relative dielectric constant. The spectral density of the small-scale ocean surface roughness, $W = W(2k_r\sin(\theta + \psi), 2k_r cos(\theta + \psi)\sin\zeta)$ [*Valenzuela*, 1978] is a function of the Bragg wavenumber and describes the shape of the radar signal that is scattered from the ocean surface. In the limit of a perfectly smooth (specular) surface, all of the scattered power is reflected away from the antenna at an angle equal to the incidence angle. A perfectly rough (Lambertian) surface scatters energy in all directions. For a plane with constant roughness, W decreases with increasing incidence angle (Bragg wavenumber).

[8] Ocean surface roughness can be described by an energy balance between the inputs due to wind and nonlinear wave-wave interactions and the losses due to viscous damping and wave breaking. The damping properties of the oil spills can be functions of the dynamic viscosity, density, surface tension, and complex dilational modulus of the contaminated ocean water [*Gade et al.*, 1998]. In the presence of a viscoelastic film, the viscous damping losses can be described by the Marangoni damping theory which predicts a resonance-type damping of the gravity waves on the ocean surface [e.g., *Alpers and Hühnerfuss*, 1988; *Gade et al.*, 1998]. The energy input from the wind is reduced in the presence of an oil spill through a reduction in the wind friction [*Fingas and Brown*, 1997] and, possibly, the surface tension [*Minchew et al.*, 2012].

[9] Reflectivity is a function of the facet tilt, radar incidence angle, and dielectric constant defined as:

$$\Gamma_{pp} = \left| \left(\frac{\sin(\theta + \psi)\cos\zeta}{\sin\theta_i} \right)^2 \alpha_{pp} + \left(\frac{\sin\zeta}{\sin\theta_i} \right)^2 \alpha_{qq} \right|^2 \tag{2}$$

where the subscript *qq* indicates either *HH* or *VV* polarizations ($p \neq q$) and the scattering coefficients, α_{HH} and α_{VV}, are [*Valenzuela*, 1968; *Valenzuela et al.*, 1971; *Valenzuela*, 1978]:

$$\alpha_{HH} = \frac{\cos\theta_i - \sqrt{\varepsilon_r - \sin^2\theta_i}}{\cos\theta_i + \sqrt{\varepsilon_r - \sin^2\theta_i}} \tag{3}$$

$$\alpha_{VV} = \frac{(\varepsilon_r - 1)\{\sin^2\theta_i - \varepsilon_r[1 + \sin^2\theta_i]\}}{\left(\varepsilon_r\cos\theta_i + \sqrt{\varepsilon_r - \sin^2\theta_i}\right)^2}. \tag{4}$$

The relative dielectric constant ε_r is taken to be:

$$\varepsilon_r = \varepsilon_r^{eff} = w_o\varepsilon_r^{oil} + (1 - w_o)\varepsilon_r^{water} \tag{5}$$

where ε_r^{water} and ε_r^{oil} are the relative dielectric constants of sea water and crude oil, respectively, and w_o is the oil weighting factor. The weighting factor is proportional to the volumetric oil concentration where the constant of proportionality is defined by the shape factor of the oil (or water) inclusions [see *Ulaby et al.*, 1986, volume 3, Appendix E].

[10] The model in equation (1) matches data at incidence angles greater than $30 - 35°$, depending on the sea state [*Minchew et al.*, 2012]. At $\theta < 30 - 35°$, equation (1) is invalid because the sensitivity of the radar signal to the small-scale roughness is low, which violates the small-perturbation assumption used to derive the model [*Valenzuela*, 1968]. Instrument noise is likely to impose an upper limit on the usable span of incidence angles [*Jones et al.*, 2011].

[11] Over the range of viable incidence angles, the co-polarized NRCS for constant tilt angles, surface roughness, and dielectric constant decreases as the incidence angle increases. It can be shown from equations (2)–(5) that the reflectivity increases with incidence angle for a constant ε_r and tilt angles, but the $\cos^4\theta_i$ term and W are dominant. When oil is present, $\sigma_{VV}^{o(oil)}/\sigma_{VV}^{o(water)}$ decreases with increasing incidence angle [e.g., *Minchew et al.*, 2012].

2.2. Inverting for w_o and W

[12] Equations (1)–(5) show that the co-polarized NRCS ratio ($\sigma^o_{HH}/\sigma^o_{VV} = \Gamma_{HH}/\Gamma_{VV}$) is a function of only the oil weighting factor and the tilt of the facets. By assuming a value for the dielectric constant of sea water, ψ and ζ can be fit using the mean co-polarized NRCS ratio for areas of relatively clean sea water. The tilt angles are governed by the long-wavelength ocean waves and, therefore, should be constant within a radar scene regardless of the presence of oil [*Minchew et al.*, 2012]. This means that we can plug ψ and ζ into the co-polarized NRCS ratio and use a simple look-up table to estimate the oil weighting factor in each pixel by assuming a value for the dielectric constant of crude oil. Plugging the estimated weighting factors and tilt angles into equations (2)–(5) yields Γ_{VV}. Finally, inverting equation (1) provides the estimated spectral density of the ocean surface roughness for each pixel. VV-polarized data is preferable to HH-polarized data because Γ_{VV} is more sensitive to w_o than Γ_{HH} and because the VV backscatter power is always greater than the HH backscatter power, giving VV a higher signal-to-noise ratio (SNR) at all incidence angles.

2.3. Oil/Water Mixing Index

[13] It is often desirable to relate estimates of the reflectivity and the surface roughness to the properties of the oil,

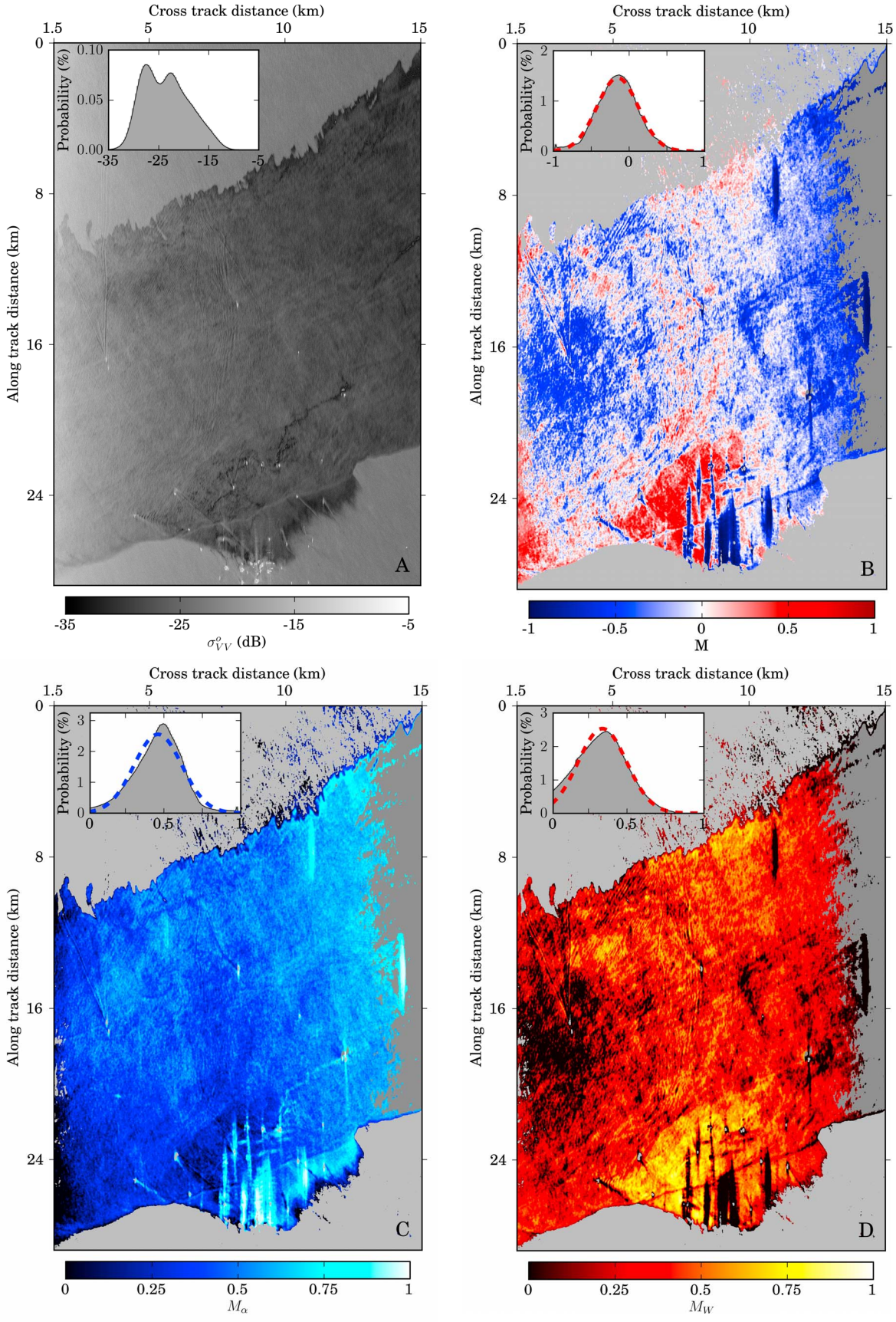
Cross track distance (km)
Along track distance (km)
Probability (%)
A
σ^o_{VV} (dB)
B
M
C
M_α
D
M_W

Figure 1

relative to the ambient sea. To that end, I propose a new oil/water mixing index (Mdex) defined as:

$$M = \frac{1}{\sigma_{VV}^{o(water)}}\left[\frac{\partial\sigma_{VV}^{o}}{\partial W}\Delta W - \frac{\partial\sigma_{VV}^{o}}{\partial\Gamma_{VV}}\Delta\Gamma_{VV}\right] \approx \frac{W^{water} - W^{oil}}{W^{water}} - \frac{\left|\alpha_{VV}^{water}\right|^2 - \left|\alpha_{VV}^{oil}\right|^2}{\left|\alpha_{VV}^{water}\right|^2} \quad (6)$$

which accounts for the difference in the relative contributions to the reduction in backscatter power from surface roughness damping and signal attenuation. In equation (6), W^{water} is the surface roughness of relatively clean water taken as close to the oil as possible (at the same incidence angle), $\left|\alpha_{VV}^{water}\right|^2$ can be calculated from equation (4) using a reasonable value of ε_r^{water}, the Δ operator indicates the difference between the relatively clean ambient water and the spilled oil, and $-1 \le M \le 1$, provided the winds in the study area are sufficient to stimulate ocean surface roughness. The first term on the right hand side of equation (6) represents the normalized damping factor M_W (0 = no damping and 1 = total damping) and the second term describes the normalized power attenuation factor M_α (0 = no attenuation and 1 = complete attenuation such that $\varepsilon_r^{eff} = 1$). M_α can be simplified using $|\alpha_{VV}|^2$ instead of Γ_{VV} because, assuming ζ is small and considering that $|\alpha_{VV}| > |\alpha_{HH}|$, equation (2) reduces to only the α_{VV} term and its leading coefficient, which cancels in the M_α ratio. It should be noted that local variations in the roughness spectrum can lead to negative values for M_W which need to be corrected prior to calculating M.

[14] Negative Mdex values indicate that the reduction of the radar backscatter power is caused more by the reduction in the total reflected power than by smoothing on the ocean surface. This means that the oil must be mixed with sea water to a depth on the order of the skin depth of the radar signal ($\delta_s = 1/k_r\left|Imag\left[\sqrt{\varepsilon_r}\right]\right|$) but with limited influence on the surface roughness. The lowest Mdex value corresponds to the limit of a high volumetric concentration of oil droplets that do not affect the surface roughness so that $W^{oil} \approx W^{water}$ and $\left|\alpha_{VV}^{oil}\right|^2 \ll \left|\alpha_{VV}^{water}\right|^2$. Areas with low Mdex values are likely to have a dark (or true) color when viewed from an aircraft (BAOAC: D), though this is dependent on the type of oil. As the Mdex value increases toward zero, the imaged area should progress toward lighter oil colors (BAOAC: T), possibly with superimposed silver, rainbow, or metallic colors (BAOAC: S, R, and M, respectively) if some of the oil is consolidated at the surface (M_W increases), or toward a natural sea water color if the oil is dispersing (M_α decreases). Skimmers might be able to recover oil that exhibits negative Mdex values [*NOAA*, 2007].

[15] Whenever the reduction in radar backscatter is caused more by the damping of the gravity-capillary surface waves the Mdex values will be positive. The condition $M \approx 1$ represents a thin film that completely damps the wind-driven waves ($W^{oil} \ll W^{water}$). Because the relative dielectric constant of oil is very low compared to sea water and radar wavelengths are on the order of centimeters, a thin film ($z_f \ll 1$ mm) will produce negligible scattering and will serve as an attenuating layer equivalent to multiplying the right side of equation (1) by $\exp\{-2z_f/\delta_s^{oil}\}$, where z_f is the thickness of the film [*Ulaby et al.*, 1986]. Therefore, a thin film on the surface will have no discernible influence on the effective dielectric constant of the scattering medium and $\left|\alpha_{VV}^{oil}\right|^2 \approx \left|\alpha_{VV}^{water}\right|^2$. These areas, known as sheens, would appear to an aerial observer as transparent, silver (BAOAC: S), rainbow (BAOAC: R), or even metallic colored (BAOAC: M) depending on their thickness. As the Mdex value decreases toward zero, the color should darken (BAOAC: T) as more oil is mixed with sea water just below the surface (M_α increases) or as patchy sheens as the surface oil breaks up (M_W decreases). Oiled areas with positive Mdex values may be recoverable with sorbents or corralled with booms and chemical herders [*NOAA*, 2007].

[16] An Mdex value of ≈ 0 over large areas could be indicative of an emulsion of sea water entrained in oil commonly called mousse [*NOAA*, 2007]. In this case the emulsion layer is thick enough and has enough heterogeneities from the sea water inclusions that the emulsion is the dominant scatterer and has a reduced dielectric constant from the high concentration of oil. This type of emulsion typically floats on the surface [*NOAA*, 2007], thereby damping the gravity-capillary surface waves. As a result, $W^{oil}/W^{water} \approx \left|\alpha_{VV}^{oil}\right|^2/\left|\alpha_{VV}^{water}\right|^2$. While mousse may be recoverable but it considerably increases the volume of contaminant that must be contained [*NOAA*, 2007]. Small areas with $M = 0$ that are bordered on either side by a film and a mixture of oil and water are not likely to contain mousse.

3. Application of the Mdex to the 2010 Deepwater Horizon Oil Spill

3.1. Data Acquisition and Processing

[17] On June 23, 2010, UAVSAR collected L-band (24-cm wavelength; 1.25 GHz; $\delta_s^{water} \sim 1$ cm) fully polarimetric SAR data over the DWH and in selected areas around the Gulf of Mexico. The day prior to the data collection, a containment cap which had been collecting oil from the wellhead for approximately one week was removed due to damage. This allowed oil to flow unfettered from the stricken well for approximately 24 hours before the data shown here were collected. Dispersants were likely applied to the area prior to the data collection, but in currently unknown quantities and locations.

[18] The oil/gas mixture that leaked from the well had to ascend $\approx$ 1500 m before reaching the surface. During the ascent, small oil droplets were detrained from the plume and remained at depth in stratified layers while larger oil droplets and gas bubbles traveled to the surface [*North et al.*, 2011]. *In situ* observations of the DWH oil swatch collected within 7 hours of the UAVSAR overflight and in the same area show that the majority of the area is covered by a brown, emulsified oil, interspersed with sheens, and an analysis of

Figure 1. Oil on sea water near the Deepwater Horizon site imaged by UAVSAR on June 23, 2010: (a) Vertically polarized NRCS σ_{VV}^{o}; (b) oil/water mixing index (Mdex) M; (c) normalized attenuation factor M_α; and (d) normalized damping factor M_W. Inset images show the PDF of the respective image and the dashed lines in Figures 1b, 1c, and 1d show the normal distribution for the equivalent mean and standard deviation. Light and dark gray areas in Figures 1b, 1c, and 1d are relatively clean water and areas with low SNR or ships, respectively, all of which are excluded from the corresponding PDF.

the UAVSAR data showed that the weighting factor w_o was between 65 and 90% [*Minchew et al.*, 2012].

[19] The UAVSAR data used in this study underwent additional processing before the inversion process described previously. To begin with, the data were averaged over 3 × 12 (cross-track × along-track) non-overlapping windows (a process known as looking) prior to public distribution to yield a spatial resolution of 5.7 m in cross-track (range) and 9.6 m in along-track (azimuth). To minimize the backscatter contamination from ships, I nulled the ship signal using the co-polarized phase difference ($\phi_{cp} = arg[S_{HH}S^*_{VV}]$, where * is the complex conjugate operator and S_{pp} relates the p-polarized transmitted and received electric fields) by considering that the return from the ocean is a single-bounce scatterer ($|\phi_{cp}| \approx 0°$) while the radar return from ships is due to double-bounce scattering ($|\phi_{cp}| \approx 180°$). Furthermore, I applied a 10 × 10 moving-average filter to the data prior to the inversions resulting in a final resolution of 57 m × 96 m. Data with $SNR < 3$ are excluded from this study and ε_r^{water} and ε_r^{oil} are taken to be $80 - i70$ [*Ulaby et al.*, 1986] and $2.3 - i0.02$ [*Folgero*, 1996; *Friiso et al.*, 1998], respectively ($i = \sqrt{-1}$).

3.2. Results

[20] The σ^o_{VV} image of the DWH site (Figure 1a) shows some variance in backscattered power within the body of the oil, evident as the large low-power area trending diagonally across the scene. The bimodal shape of the probability density function (PDF; inset of Figure 1a) indicates that values of σ^o_{VV} over the oil are typically 5 dB less than the values over water. An area of lower backscatter power is evident in the bottom center of the oil and some ships can be seen traversing the polluted water leaving wakes that mark their path. The high backscatter area running the length of the left side of the image is an artifact of radar imaging (higher backscatter is expected at near-range) and the sharp edge at the lower side of the oil is indicative of bunching from wind, which at the time of the data collection was blowing approximately anti-parallel to the aircraft's flight path (i.e. up in Figure 1). The DWH site is located at the bottom center of the oil swatch in the area with numerous high-backscatter points identified as ships.

[21] The Mdex map (Figure 1b) reveals a more heterogeneous oil region than is evident in the σ^o_{VV} image. Patterns in the Mdex map are consistent with those seen in near-coincident aerial photographs [*Jones et al.*, 2011; *Minchew et al.*, 2012]. The longer narrow bands of positive Mdex values are streamers [*NOAA*, 2007] while the relatively large region of positive Mdex values near the bottom of the image is a sheen whose proximity to the DWH site suggests that it is at or near the location where the plume met the surface of the water. The vertically oriented areas of very low Mdex values at the bottom of the image are attributable to the impulse sidelobes of the ships in this area, and other vertical streaks of low Mdex values are image artifacts likely due to radio frequency interference.

[22] The Mdex PDF (inset of Figure 1b), which considers only areas identified as oil, indicates a Gaussian distribution (dashed line) with a mean of ≈ -0.21 and standard deviation of ≈ 0.27. This distribution indicates that the majority of the spilled oil that was close to the surface near the DWH site was mixed with sea water to a depth of at least a few millimeters. Comparing the spatial patterns in the M_α and M_W images (Figures 1c and 1d, respectively) shows that most of the heterogeneity in the Mdex map is due to high frequency changes in the surface roughness. The same spatial variance of surface roughness is not observed in the relatively clean water surrounding the oil, indicating that the viscoelastic properties of oil can vary substantially on spatial scales of order 100 m. The M_W PDF of only oiled areas clearly deviates from a Gaussian distribution (dashed line in inset of Figure 1d) at lower values indicating that a large amount of oil in this image is entrained in the water column rather than on the surface in viscoelastic films.

[23] The distribution of M_α values for oil shows that the oil swatch near the DWH site is continuous on the scale of the image resolution because any patches of relatively clean water within the oil must have $M_\alpha \approx 0$. The M_α PDF is approximately Gaussian-distributed (Figure 1c inset) with a mean near 0.45, corresponding to $w_o \approx 80 - 85\%$, and a standard deviation of ≈ 0.15. The small variance of w_o likely indicating that the volumetric concentration of oil varies only slightly over the study area.

4. Conclusion

[24] SAR can provide useful information on oil characteristics as long as the reduction in the total radar backscatter power can be decoupled from the damping of the small scale roughness of sea surface. I demonstrated a method for decoupling these effects using co-polarized SAR data and applied a simple classification scheme, the Mdex, to data collected by UAVSAR on June 23, 2010 near the DWH site. The results indicate that the majority of oil at or near the surface was mixed with sea water to a depth of at least a few millimeters. Small-scale features, such as streamers, are evident in the Mdex values but not in the NRCS values. High frequency spatial variations in the damping properties of oil on the wind-driven ocean surface roughness are also prevalent while the volumetric concentration of oil appears to vary only slightly across the image.

[25] **Acknowledgments.** I would like to thank Bryan Riel, Cathleen Jones, Ben Holt, and Jakob van Zyl for the many informative discussions on this topic. The raw UAVSAR data were processed at the Jet Propulsion Laboratory and archived under the name gulfco_14010_10054_100_100623 by the Alaska Satellite Facility.

[26] The Editor thanks two anonymous reviewers for their assistance in evaluating this paper.

References

Alpers, W., and H. Hühnerfuss (1988), Radar signatures of oil films floating on the sea surface and the Marangoni effect, *J. Geophys. Res.*, *93*(C4), 3442–3648.

Brekke, C., and A. Solberg (2008), Classifiers and confidence estimation for oil spill detection in ENVISAT ASAR images, *IEEE Geosci. Remote Sens. Lett.*, *5*(1), 65–69.

Fingas, M., and C. Brown (1997), Review of oil spill remote sensing, *Spill Sci. Technol. Bull.*, *4*(4), 199–208.

Fiscella, B., A. Giancaspro, F. Nirchio, P. Pavese, and P. Trivero (2000), Oil spill detection using marine SAR images, *Int. J. Remote Sens.*, *21* (18), 3561–3566.

Folgero, K. (1996), Bilinear calibration of coaxial transmission/reflection cells for permittivity measurement of low-loss liquids, *Meas. Sci. Technol.*, *7*(9), 1260–1269.

Friiso, T., Y. Schildberg, O. Rambeau, T. Tjomsland, H. Fordedal, and J. Sjoblom (1998), Complex permittivity of crude oil and solutions of heavy crude oil fractions, *J. Dispersion Sci. Technol.*, *19*(1), 93–126.

Gade, M., W. Alpers, H. Hühnerfuss, V. Wismann, and P. Lange (1998), On the reduction of the radar backscatter by oceanic surface films:

Scatterometer measurements and their theoretical interpretation, *Remote Sens. Environ.*, *66*, 52–70.

Jones, C. E., B. Minchew, B. Holt, and S. Hensley (2011), Studies of the Deepwater Horizon oil spill with the UAVSAR radar, in *Monitoring and Modeling of the Deepwater Horizon Oil Spill: A Record-Breaking Enterprise*, *Geophys. Monogr. Ser.*, vol. 196, edited by Y. Liu et al., pp. 33–50, AGU, Washington D. C.

Minchew, B., C. Jones, and B. Holt (2012), Polarimetric analysis of backscatter from the Deepwater Horizon oil spill using L-band synthetic aperture radar, *IEEE Trans. Geosci. Remote Sens.*, *99*, 1–19.

National Research Council (2003), *Oil in the Sea III: Inputs, Fates, and Effects*, Natl. Acad. Press, Washington, D. C.

NOAA (2007), Open water oil identification job aid for aerial observation, Off. of Response and Restoration, Silver Spring, Md. [Available at http://response.restoration.noaa.gov/jobaid/orderform.]

North, E. W., E. E. Adams, Z. Schlag, C. R. Sherwood, R. He, K. H. Hyun, and S. A. Socolofsky (2011), Simulating oil droplet dispersal from the Deepwater Horizon spill with a Lagrangian approach, in *Monitoring and Modeling of the Deepwater Horizon Oil Spill: A Record-Breaking Enterprise*, *Geophys. Monogr. Ser.*, vol. 196, edited by Y. Liu et al., pp. 217–226, AGU, Washington D. C.

Solberg, A., G. Sotrvik, R. Solberg, and E. Volden (1999), Automatic detection of oil spills in ERS SAR images, *IEEE Trans. Geosci. Remote Sens.*, *37*(4), 1916–1924.

Ulaby, F. T., R. K. Moore, and A. K. Fung (1986), *Microwave Remote Sensing: Active and Passive*, Artech, Dedham, Mass.

Valenzuela, G. R. (1968), Scattering of electromagnetic waves from a tilted slightly rough surface, *Radio Sci.*, *3*, 1057–1066.

Valenzuela, G. R. (1978), Theories for the interaction of electromagnetic and ocean waves—A review, *Boundary Layer Meteorol.*, *13*, 61–85.

Valenzuela, G. R., M. B. Laing, and J. C. Daley (1971), Ocean spectra for the high frequency waves as determined from airborne radar measurements, *J. Mar. Res.*, *29*, 69–84.

Wright, J. (1966), Backscattering from capillary waves with application to sea clutter, *IEEE Trans. Antennas Propag.*, *14*(6), 749–754.